Genetic Ablation of the Cystine Transporter xCT in PDAC Cells Inhibits mTORC1, Growth, Survival, and Tumor Formation via Nutrient and Oxidative Stresses

Boutaina Daher[1], Scott K. Parks[1], Jerome Durivault[1], Yann Cormerais[1], Hanane Baidarjad[1], Eric Tambutte[2], Jacques Pouysségur[1,3], and Milica Vučetić[1]

Abstract

Although chemoresistance remains a primary challenge in the treatment of pancreatic ductal adenocarcinoma (PDAC), exploiting oxidative stress might offer novel therapeutic clues. Here we explored the potential of targeting cystine/glutamate exchanger (*SLC7A11*/xCT), which contributes to the maintenance of intracellular glutathione (GSH). Genomic disruption of xCT via CRISPR-Cas9 was achieved in two PDAC cell lines, MiaPaCa-2 and Capan-2, and xCT-KO clones were cultivated in the presence of N-acetylcysteine. Although several cystine/cysteine transporters have been identified, our findings demonstrate that, *in vitro*, xCT plays the major role in intracellular cysteine balance and GSH biosynthesis. As a consequence, both xCT-KO cell lines exhibited amino acid stress with activation of GCN2 and subsequent induction of ATF4, inhibition of mTORC1, proliferation arrest, and cell death. Tumor xenograft growth was delayed but not suppressed in xCT-KO

cells, which indicated both the key role of xCT and also the presence of additional mechanisms for cysteine homeostasis *in vivo*. Moreover, rapid depletion of intracellular GSH in xCT-KO cells led to accumulation of lipid peroxides and cell swelling. These two hallmarks of ferroptotic cell death were prevented by vitamin E or iron chelation. Finally, *in vitro* pharmacologic inhibition of xCT by low concentrations of erastin phenocopied xCT-KO and potentiated the cytotoxic effects of both gemcitabine and cisplatin in PDAC cell lines. In conclusion, our findings strongly support that inhibition of xCT, by its dual induction of nutritional and oxidative cellular stresses, has great potential as an anticancer strategy.

Significance: The cystine/glutamate exchanger xCT is essential for amino acid and redox homeostasis and its inhibition has potential for anticancer therapy by inducing ferroptosis.

Introduction

Despite great efforts to improve diagnostic strategies, surgical procedures and chemotherapeutic regiments, the overall prognosis for patients with the most aggressive malignancies such as pancreatic ductal adenocarcinoma (PDAC) remains alarmingly poor (1). Although the cause of poor patient prognosis are wide ranging, a main problem is the lack of the adequate treatment and/or resistance to conventional chemotherapeutic approaches.

Increased glutathione (GSH) levels and GSH-dependent biotransformation in many tumors increases resistance to chemotherapy and radiotherapy enabling tumor cells to exhibit characteristic cancer hallmarks (2, 3). Although GSH has been recognized for a long time as a potential target for anticancer therapy, recent contextualization of the specific, lipid peroxide-dependent cell death termed ferroptosis (4) has shed new light on the importance of GSH for cancer cells. Namely, increased production of reactive oxygen species (mild pro-oxidative state) in cancer cells (5) leads to oxidative damage of different biomolecules, including polyunsaturated fatty acids in cell membranes (lipid peroxidation). This oxidative event is threatening to the permeability and fluidity of the membrane lipid bilayer, and thus, for cell integrity and survival (6). The key player in preventing ferroptotic cell death is GSH peroxidase 4 (GPx4), a selenocysteine (Se-CySH)-containing protein (7), which converts lipid peroxides (LOOH) into nontoxic lipid alcohols using GSH as reducing power (8). Stockwell's group showed that depletion of the GSH intracellular pool or downregulation of GPx4 activity leads to accumulation of membrane LOOH, which are responsible for the characteristic ferroptotic cell death that can be prevented by lipophilic antioxidants such as vitamin E (4, 7). Interestingly, these data and other studies unambiguously showed that the intracellular GSH pool in cancer cells is almost exclusively determined by the import of the oxidized form of cysteine (cystine, CySSCy) from the extracellular space through the system xc⁻ that serves as CySSCy/Glu antiporter (4, 9–12).

[1]Medical Biology Department, Centre Scientifique de Monaco (CSM), Monaco.
[2]Marine Biology Department, Centre Scientifique de Monaco (CSM), Monaco.
[3]University Côte d'Azur, Institute for Research on Cancer & Aging (IRCAN), CNRS, INSERM, Centre A. Lacassagne, Nice, France.

Note: Supplementary data for this article are available at Cancer Research Online (http://cancerres.aacrjournals.org/).

Current address for Y. Cormerais: Department of Genetics and Complex Diseases, Harvard School of Public Health, Boston, MA.

Corresponding Authors: Jacques Pouysségur, IRCAN, University of Côte d'Azur, 33 Avenue Valombrose, Nice 06189, France. Phone: 3368505 4881; Fax: 33492 03 1225; E-mail: jacques.pouyssegur@unice.fr and Milica Vučetić, Centre Scientifique de Monaco, Medical Biology Department, 8 Quai Antoine 1er 98000 Monaco, Phone: 377-97-77-44-21; E-mail: milica@centrescientifique.mc

AACR 3877

System xc$^-$, consisting of a substrate-specific subunit xCT (*SLC7A11*) and its chaperone CD98 (*SLC3A2*), functions as a Na$^+$-independent, electroneutral exchange system for CySSCy and Glu (13). It has been reported that xCT, together with L-type amino acid transporter 1 (LAT1/*SLC7A5*) and alanine–serine–cysteine transporter 2 (ASCT2/*SLC1A5*), comprise the "minimal set" of transporters required for cancer amino acid (AA) homeostasis and this group is known to be highly upregulated in cancer (14–16). Previously, we and others have shown that disruption/inhibition of either LAT1 or ASCT2 strongly affects AA balance and thus tumor cell growth both *in vitro* and *in vivo* (17–21). In this study, we investigated the importance of xCT in PDAC cells along with the role of this transporter in response to chemotherapeutic agents (gemcitabine and cisplatin) via its genomic disruption in 2 different primary PDAC cell lines—MiaPaCa-2 and Capan-2 using CRISPR-Cas9. Our results revealed that disruption of the xCT gene in both cell lines induced a marked AA stress response revealed by ATF4 and GCN2 kinase activation, suppressing proliferation and survival capacity. Interestingly, *in vivo* tumor xenograft growth was delayed but not suppressed in xCT-KO cells, which indicated both the key role of xCT and also the presence of additional mechanisms of cysteine homeostasis *in vivo*. The characteristic *in vitro* phenotype of xCT-KO seems to be driven by a complete collapse of cellular GSH levels following N-acetylcysteine (NAC) removal, leading to the accumulation of membrane lipid peroxides and cell swelling. These hallmarks of ferroptotic cell death were prevented by vitamin E (lipophilic antioxidant) or Fe^{2+} chelation (deferoxamine, DFO). Finally, *in vitro* pharmacologic inhibition of xCT by erastin (1 μmol/L) phenocopied xCT-KO and potentiated the cytotoxic effects of both gemcitabine and cisplatin in both PDAC cell lines. Combined, our results suggest that inhibition of xCT, and thereby induction of nutritional and oxidative cellular stresses is a plausible strategy for sensitization of PDAC tumors to ferroptosis.

Materials and Methods

Cell culture

Human PDAC MiaPaCa-2 and Capan-2 cells were kindly provided by Dr. Sophie Vasseur (CRCM, Marseille, France), who obtained them from ATCC, and authenticated in 2015. They were routinely tested for *Mycoplasma* (PlasmoTest Mycoplasma Detection Kit; InvivoGen) and cultivated up to 10th passage. Cells were grown at 37°C/5% CO$_2$ in DMEM (Gibco) supplemented with 7.5% FBS, penicillin (10 U/mL), and streptomycin (10 μg/mL). *SLC7A11* deleted cell lines were maintained and experiments were conducted in the same media supplemented with 1 mmol/L NAC (Sigma-Aldrich) or 1 μmol/L vitamin E (α-tocopherol; Sigma-Aldrich).

Genomic disruption of xCT using CRISPR-Cas9 and xCT rescue

MiaPaCa-2 and Capan-2 wild-type (WT) cells were transfected with PX458 plasmids containing CRISPR-Cas9 targeting regions of the fourth and fifth exon of the xCT (*SLC7A11*) gene using Nucleofection (Lonza). As the PX458 plasmid contains GFP, single-cell sorting was conducted (24-hour posttransfection) using BD FACSAria (BD Biosciences), individual clones were cultivated in presence of 1 mmol/L NAC, and subsequently analyzed for xCT expression by immuno-

blotting. xCT cDNA (plasmid obtained from M. Palacin, IRB, Barcelona, Spain) was used to restore the xCT function in xCT-KO clones from both cell lines with xCT WT cells being used as a control.

Induction of xCT expression

MiaPaCa-2 and Capan-2 WT and xCT-negative clones were seeded in DMEM supplemented with NAC for 24 hours and the next day media was removed, cells were washed 2 times with PBS and treated with 20 (MiaPaCa-2) or 30 (Capan-2) μmol/L JPH203 inhibitor (kindly provided by Dr H. Endou, Department of Pharmacology and Toxicology, Kyorin University School of Medicine, Tokyo, Japan, and Dr M. Wempe, Department of Pharmaceutical Sciences, School of Pharmacy, University of Colorado Denver Anschutz Medical Campus, Aurora, CO) in Ham's F-12 nutrient media (Gibco) supplemented with 7.5% dialyzed serum during 48 hours, after which, the xCT immunoblotting was repeated.

Proliferation assay

The different cell lines (2.5×10^4 cells) were seeded onto 6-well plates in triplicate per cell line and per condition. We measured proliferation by trypsinization and counting daily (Coulter Z1; Beckman) during 7 days. The cell proliferation index was calculated as "fold of change" by standardizing each measurement to the cell number obtained 24 hours after seeding (day 0).

Clonogenicity assay

The different cell lines (1,000 cells per dish) were seeded in 60 mm dishes in triplicate per cell line and per condition and incubated at 37°C, 5% CO$_2$. After 7 to 17 days dishes were stained with 5% Giemsa (Fluka) for 30 to 45 minutes to visualize colonies.

Immunoblotting

Cells were lysed in 1.5 × Laemmli buffer, and protein concentrations were determined using the Pierce BCA protein assay (Thermo Fisher Scientific). Protein extracts (20–40 μg) were separated by electrophoresis on 10% SDS-polyacrylamide gel and transferred onto polyvinylidene difluoride membranes (Millipore). Membranes were blocked in 5% nonfat milk in TN buffer (50 mmol/L Tris-HCl, pH 7.4, 150 mmol/L NaCl) and incubated with the following antihuman antibodies: rabbit xCT (1:1,000, 12691; Cell Signaling Technology), mouse GCN2 (1:250, sc-374609; Santa Cruz Biotechnology), mouse phospho-GCN2 (1:500, ab75836; Abcam), rabbit EIF2α (1:1,000, ab5369; Abcam), mouse phospho-EIF2α (1:1,000, ab32157; Abcam), rabbit ATF4 (1:1,000, 11815S; CST), rabbit S6K1 (1:1,000, 9202S; CST), rabbit phospho-S6K1 (1:1,000, 9202S; CST), rabbit RPS6 (1:1,000, 2217S; CST), rabbit phospho-RPS6 (1:1,000, 2215S; CST), rabbit NRF2 (1:1,000, ab137550; Abcam), rabbit vimentin (1:1,000, 5,741; CST), and mouse E-cadherin (1:1,000, 14472; CST). Detection of tubulin/actin/ARD1 was used as a protein loading control (1:10,000 MA5-16308/1:5,000 MA5-15739; Thermo Scientific, homemade; ref. 22). Immunoreactive bands were detected with horseradish peroxidase antimouse or antirabbit antibodies (Promega) using the ECL system (Merck Millipore; WBKLS0500). Immunoblot analysis was performed using the LI-COR Odyssey Imaging System.

Uptake of radioactive-labeled cystine

Cells (2.5×10^5) were seeded onto 35-mm dishes, in duplicate per cell line. Twenty-four hours after seeding, cells were treated with JPH203 inhibitor in Ham's F-12 media (in order to maximize the expression of the xCT) during following 48 hours. Culture media were removed and cells were carefully washed with prewarmed Na^+-free Hank's Balanced Salt Solution (HBSS: 125 mmol/L choline chloride, 4.8 mmol/L KCl, 1.2 mmol/L $MgSO_4$, 1.2 mmol/L KH_2PO_4, 1.3 mmol/L $CaCl_2$, 5.6 mmol/L glucose, and 25 mmol/L HEPES), preincubated in 1.0 mL of prewarmed Na^+-free HBSS at 37°C for 5 minutes before adding substrates for the uptake experiment. Cells were then incubated at room temperature for 5 minutes in 1 mL of Na^+-free HBSS containing L-$[3,3`-^{14}C]$-cystine (0.2 µCie/mL; PerkinElmer) and 50 µmol/L cold cystine (Sigma-Aldrich). Subsequently, cells were washed 3 times with Na^+-free HBSS containing 10 mmol/L glutamate (Sigma-Aldrich) as a natural inhibitor of xCT. Cells were then lysed with 1 mL of 1 mol/L NaOH and mixed with 12 mL of Emulsifier-Safe cocktail (PerkinElmer). Radioactivity was measured using a β-scintillation counter. Relative L-$[^{14}C]$-cystine uptake was normalized by the protein content.

Cell death assay

Different cell lines were seeded in 12-well plate (50,000–150,000 cells per well, triplicate per condition) at 37°C/5% CO_2 in DMEM supplemented or not with 1µmol/L vitamin E, and the cell death is measured after 24, 48, 72, and 96 hours based on propidium iodide (PI) staining method using ADAM-MC Automatic Cell Counter (AlphaMetrix Biotech).

GSH measurement

Cells (40,000 per well, triplicate per condition) were seeded in 96-well plate at 37°C/5% CO_2 in DMEM supplemented with 1 µmol/L vitamin E, 0.2 mmol/L NAC, or 1 mmol/L NAC. Intracellular GSH level was determined after 24 and 48 hours by SAFAS Xenius XOF (Safas) using a GSH fluorimetric Assay Kit (CS1020; Sigma) according to manufacturer's instructions. Relative GSH content was normalized to the number of cells.

Chemotherapy

MiaPaCa-2 and Capan-2 WT cells were seeded in 60 mm dishes (50,000–150,000 cells per dish) at 37°C/5% CO_2 in DMEM and after 24 hours from seeding cells were treated with erastin (Sigma-Aldrich), gemcitabine (Hospital Pasteur, Nice, France), cisplatin (Sigma-Aldrich), or combination of erastin and gemcitabine/cisplatin. Two days after cells were analyzed for cell death by flow cytometry.

Flow cytometry

Experiments were performed at least 3 times, 10,000 cell events were analyzed per sample using a BD FACSMelody cytometer and data were analyzed using FlowJo software.

Cell death: Cells were collected by trypsinization, merged with the corresponding supernatant and centrifuged. Cell pellets were resuspended in FACS buffer (PBS, 0.2% BSA, 2 mmol/L EDTA) and stained with 2 µg/mL PI (Invitrogen). PI was added just before analysis.

Detection of lipid peroxides: BODIPY 581/591 C11 (Molecular Probes) dye was added in the media to the final concentration of 2 µmol/L and cells were incubated for 30 minutes at 37°C/5% CO_2 protected from the light. Subsequently, cells were washed 2 times with PBS, detached using accutase (Dutscher), and resuspended in FACS buffer. For data presentation the modal scaling option was used (each peak is normalized to its mode, i.e., to % of maximal number of cells found in a particular bin).

Tumor xenograft studies

Animal care and housing were done in compliance to the EU directive 2010/63/EU. Briefly, each cage contained 5 mice with an enriched environment. Food and water were given *ad libitum*, and the litter was changed on a weekly basis. The animal experimental protocol was approved by the local animal care committee (Veterinary Service and Direction of Sanitary and Social Action of Monaco; Dr. H. Raps, Centre Scientifique de Monaco, Monaco). The different MiaPaCa-2 and Capan-2 stable cell lines (1×10^6 cells), suspended in 300 µL of high protein concentration Matrigel (Corning; Thermo Fisher Scientific) and serum-free DMEM (final protein concentration 8 mg/mL) supplemented with insulin–transferrin–selenium (Life Technologies) and 1 µmol/L vitamin E, were injected subcutaneously into the back of 8-week-old female athymic mice (Janvier) on the left and right side. Tumor dimensions were measured 2 to 3 times a week using calipers, and the tumor volume was determined by using the formula: $(4\pi/3) \times L/2 \times W/2 \times H/2$ (L, length; W, width; and H, height). When the tumor volume reached 1,000 to 1,500 mm^3, mice were euthanized. After 26 days of cells injection two Matrigel plugs with MiaPaCa-2 xCT-KO cells were removed for cell extraction. The plugs were homogenized and suspended in DMEM media supplemented with 7.5% FBS, penicillin (20 U/mL), streptomycin (20 µg/mL), and 1 mmol/L NAC.

Statistical analysis

Data are expressed as mean ± SEM. Each experiment was performed at least 3 times. Statistical analysis was done with the unpaired Student t test. Differences between groups were considered statistically significant when $P < 0.05$.

Results

xCT is the predominant transporter of cystine (CySSCy) in two independent PDAC cell lines and its disruption completely abolishes growth

xCT knockouts (KO) were obtained in MiaPaCa-2 and Capan-2 PDAC cell lines using CRISPR-Cas9. Because xCT expression can be low in *in vitro* cell culture, xCT-KO confirmation via Western blot analysis was assessed under conditions that increase xCT expression. We used a LAT1 inhibitor (JPH203) for 24 hours (MiaPaCa-2) and 48 hours (Capan-2) to increase amino acid stress (Fig. 1A). The AA-stress response activates the GCN2-ATF4 cascade and consequently induces expression of all genes containing ATF4 response promoter elements (including xCT; refs. 17, 23). As JPH203 is a competitive inhibitor of LAT1 (24), we used Ham's F-12 nutrient media containing lower concentration of L-leucine in comparison with standard DMEM media (131 µmol/L vs. 800 µmol/L), to increase inhibitor efficiency. Indeed, the treatment of both WT and xCT-KO cells induced strong activation of GCN2 kinase, which consequently led to increased expression of xCT in WT cells (Fig. 1A). The xCT band was not detected in xCT-KO clones and subsequent experiments were performed on two independent clones
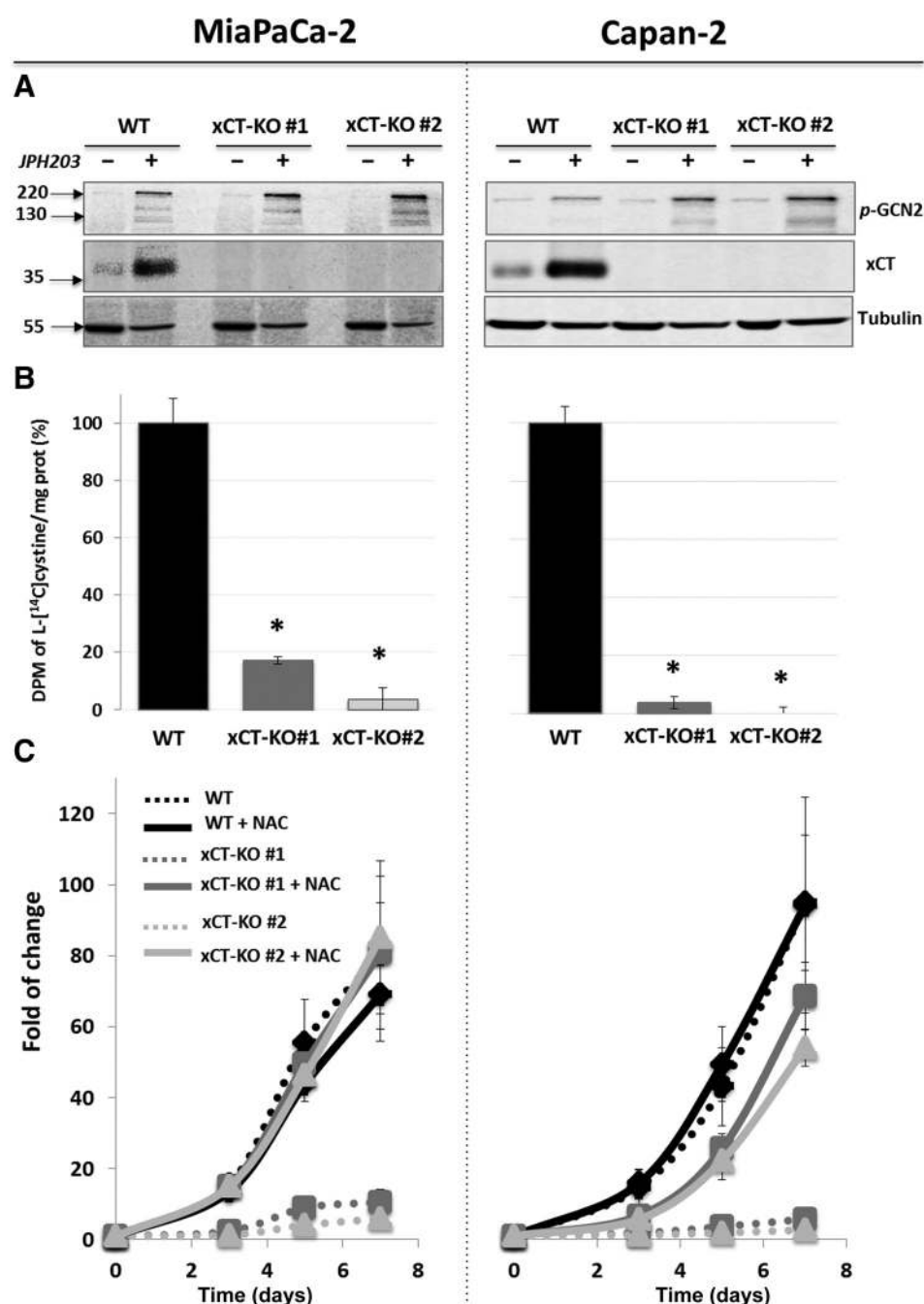
MiaPaCa-2   Capan-2

Figure 1

xCT is a main CySSCy transporter in two PDAC cell lines and its invalidation dramatically reduces proliferation. **A,** xCT expression was analyzed in MiaPaCa-2 and Capan-2 WT and two independent clonal cell lines of xCT-KO (#1 and #2). To maximize the expression of xCT, cells were treated with the specific inhibitor of LAT1 (JPH203; for more details, refer to Materials and Methods). Three independent experiments were performed and representative blots are shown. Tubulin was used as a loading control. **B,** xCT transport activity of MiaPaCa-2 and Capan-2 WT, and xCT-KO cells was measured by L-(3,3′-^{14}C)-cystine (^{14}C-cystine) uptake in Na$^+$-free HBSS media containing 50 μmol/L cold cystine. These results represent the average ± SEM; $n = 2$. **C,** Proliferation of WT and xCT-KO cells of two cell lines in the presence and absence of 1 mmol/L NAC. Proliferation rates are presented as fold of change (mean ± SEM; $n = 3$). *, $P < 0.05$, comparison with WT control cells.

to minimize clonal heterogeneity. Analysis of genomic DNA and sequencing of the CRISPR-targeted site demonstrated disruptive mutations in the *SLC7A11* gene (Supplementary Table S1) that caused the lack of corresponding protein expression (Fig. 1A).

Because CySSCy/CySH have been described to be imported into the cell via different transporters (25), we investigated the importance of xCT for overall CySSCy uptake. The glutamate-sensitive ^{14}C-CySSCy uptake assayed in WT cells was reduced by ∼90% in both PDAC xCT-KO cell lines (Fig. 1B), demonstrating the main role of xCT in CySSCy uptake.

In both PDAC cell lines, cultivated in the absence of NAC, xCT-deletion significantly reduced the proliferation and clonogenicity potential. More precisely, proliferation of xCT-KO cell lines was completely suppressed in DMEM media during 7 days (Fig. 1C, dashed lines). Also, no visible clones were detected after 10 days in clonogenicity assays of xCT-KO cells (Supplementary Fig. S1A). Conversely, the effects of the genetic disruption of xCT was reverted by the addition of the cysteine donor NAC (1 mmol/L) that is able to diffuse across the plasma membrane (Fig. 1C, full lines; ref. 26). Clonogenicity potential of xCT-KO cells was reverted not only

Figure 2

Genetic disruption of xCT in MiaPaCa-2 cells results in massive ferroptotic cell death with protection via NAC or the lipophilic antioxidant vitamin E supplementation. **A,** Cell viability was measured using the PI staining method (see Materials and Methods). Cells were seeded in DMEM supplemented or not with 1 μmol/L vitamin E (α-tocopherol), and cell viability was analyzed after 24, 48, 72, and 96 hours. These results represent the average of three independent experiments ± SEM. *, $P < 0.05$, comparison with WT control cells. **B,** To investigate a hallmark of ferroptosis, lipid peroxides were measured 24-hour postseeding in MiaPaCa-2 WT and xCT-KO cells in DMEM supplemented or not with 1 μmol/L vitamin E/1 mmol/L NAC using the redox-sensitive dye BODIPY 581/591 C11. Presented histograms are representative of three independent experiments. **C,** Characteristic morphology of dying MiPaCa-2 and Capan-2 xCT-KO clones one day following NAC removal.
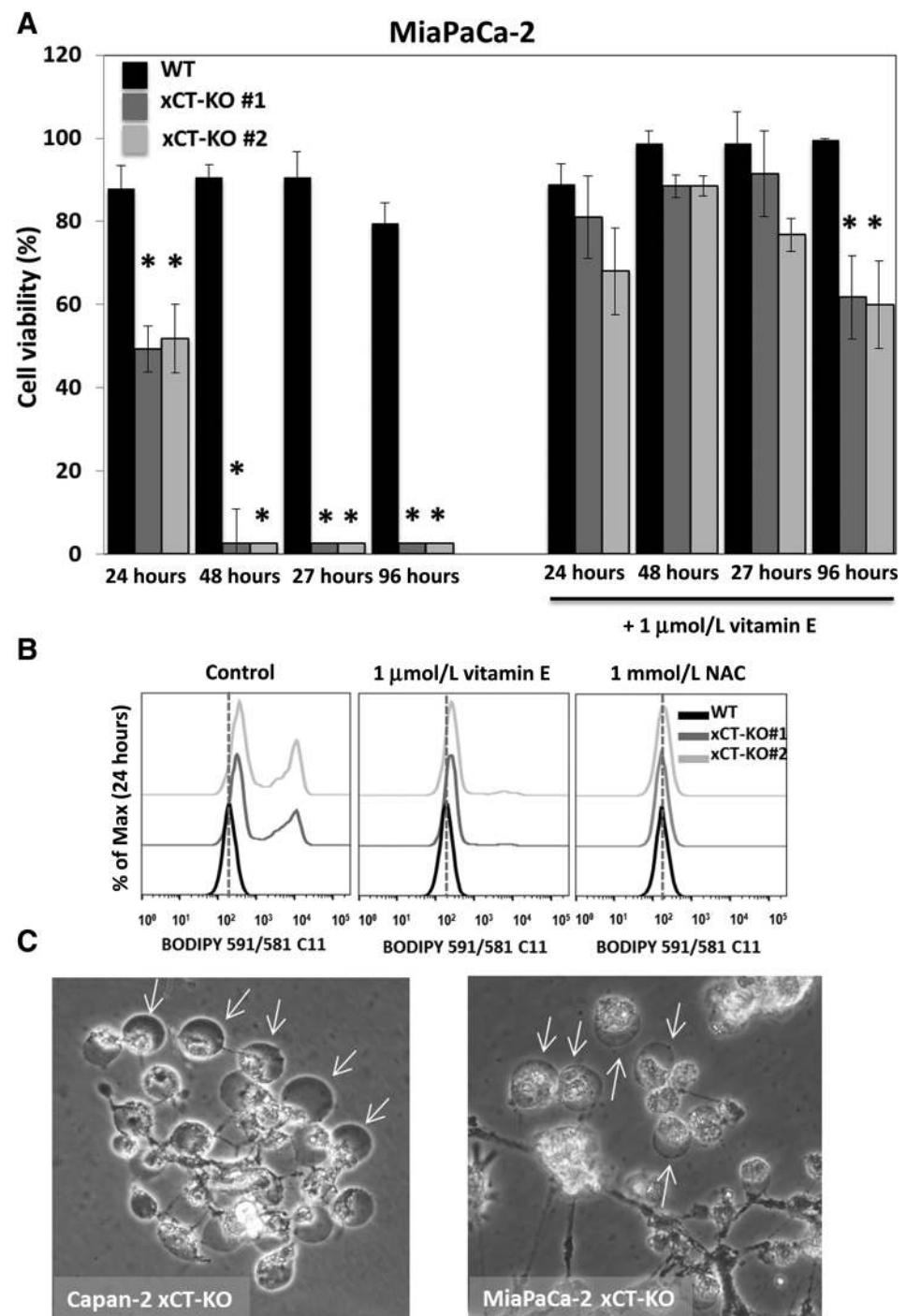
by NAC (Supplementary Fig. S1A), but also β-mercaptoethanol and GSH (Supplementary Fig. S1B). Finally, expression of xCT cDNA in both PDAC cell lines fully restored their WT phenotypes, excluding any off-target effects resulting from CRISPR-Cas9 selection (see Supplementary Fig. S1C for MiaPaCa-2 cell line).

Genetic disruption of xCT causes accumulation of membrane lipid peroxides and consequent induction of ferroptotic cell death in both PDAC cell lines

As the disruption of xCT completely suppressed PDAC cell proliferation (unless NAC was added), we analyzed the impact of xCT-KO on cell survival (Fig. 2A; Supplementary Fig. S2A).

Observation of MiaPaCa-2 xCT-KO cells 24-hour postseeding revealed an approximately 50% reduction in viability, whereas near 100% mortality was observed by 48-hour postseeding (Fig. 2A, left). A similar impact and relatively slower time course on loss of viability was observed for Capan-2 xCT-KO cells (Supplementary Fig. S2B, gray lines). According to previous work, pharmacologic inhibition of xCT is related to a specific type of cell death termed "ferroptosis" (4, 9–12). One of the main molecular characteristics of this type of cell death is the accumulation of membrane lipid peroxides that can be prevented by vitamin E supplementation or iron chelation (4). First, we found that 1 µmol/L of the antioxidant vitamin E, as well as 100 µmol/L of the iron chelator—DFO, indeed prevented cell death (Fig. 2A, right side and Supplementary Fig. S2C, respectively). The same was observed in clonogenicity assays upon substitution of NAC with either vitamin E or DFO for 24 hours (Supplementary Fig. S2D). Second, utilization of a specific dye for lipid peroxides revealed a strong increase in the time-frame preceding detection of massive cell death after seeding MiaPaCa-2 xCT-KO, a feature that was also abolished by vitamin E or NAC (Fig. 2B, gray lines). The characteristic feature of ferroptotic cell death, a rapid cell swelling before cell disruption, was noticed in both xCT-disrupted cell lines (Fig. 2C). Twenty-four hours upon removal of NAC, a characteristic cell swelling in which the entire cellular content had been concentrated away from the cell periphery was observed (Fig. 2C; Supplementary Fig. S2D). The dramatic cell swelling and subsequent death was suppressed by vitamin E, NAC, or Fe^{2+} chelation (Supplementary Fig. S2D).

The protective effect of vitamin E was further confirmed by clonogenicity assays, where cells were seeded initially ± vitamin E, and each subsequent day, proliferation of one set of the WT and xCT-KO cells were exposed to NAC supplementation. NAC addition succeeded to consistently rescue xCT-KO cell clonogenicity only if cells were pretreated with vitamin E and to a maximum of 2 days in the absence of NAC (Supplementary Fig. S3A).

Combined, our findings demonstrate unambiguously that xCT disruption in both PDAC cell lines induces a dramatic oxidative stress that precipitates cell death via ferroptosis.

xCT is fundamental for cysteine homeostasis and antioxidant capacity in PDAC cell lines

As cellular cysteine availability is a limiting factor for synthesis of the antioxidant GSH, we explored the effect of xCT-KO and suppressed CySSCy uptake (Fig. 1B) on the cellular GSH pool. xCT-KO cells showed a complete collapse of intracellular GSH at 24 hours after seeding in the absence of NAC (Fig. 3A), demonstrating that, in this *in vitro* context, only xCT is capable of providing sufficient cellular cysteine. Interestingly, NAC supplementation corresponding to the usual cyst(e)ine concentration found in DMEM (0.2 mmol/L) increased GSH levels in xCT-KO cells, but not to control levels. However, when NAC supplementation was increased to 1 mmol/L, GSH levels were completely restored to control levels.

Next, we analyzed the effect of xCT disruption on the 2 main AA-sensing pathways: GCN2 and mTORC1 (reviewed in ref. 27; Fig. 3B; Supplementary Fig. S3B). The effects of NAC and vitamin E on the AA balance of xCT-KO cells were also estimated. In xCT-KO cells ± vitamin E supplementation, both phospho-GCN2 and the transcriptional factor ATF4 were strongly upregulated after 24 hours (MiaPaCa-2; Fig. 3B) and 48 hours (Capan-2; Supplementary Fig. S3B). The GCN2 downstream effector protein

eIF2 was also induced. On the contrary, members of the mTORC1-signaling pathway, S6 kinase 1 (S6K1) and ribosomal S6 protein (S6RP), were both substantially downregulated (measured as a decrease in phosphorylation status) under these same conditions in comparison with corresponding NAC-treated groups. Addition of NAC, at either 1 or 3 mmol/L concentrations, reversed the induction of the AA-sensing pathways in xCT-KO cells. Interestingly, the level of p-S6K1 and p-S6RP in NAC-treated xCT-KO cells seems to be higher than in corresponding WT cells although no other different phenotype characteristic (proliferation, content of lipid peroxide, clonogenicity potential, etc.) were observed between these cells. This suggests that different homeostatic states (with regards to mTORC1) in these cells are achieved upon NAC treatment in comparison with WT cells. WT cells were unaffected in all conditions tested. In conclusion, besides the major oxidative lethal stress, xCT disruption induces an additional nutritional stress.

Considering the dual role of cysteine in the cell (proteinogenic and redox), we compared phenotypic characteristics of Capan-2 xCT-KO cells with their counterparts missing the catalytic subunit of the main enzyme involved in GSH biosynthesis–glutamyl-cysteine ligase (GCLc-KO). GSH levels in Capan-2 GCLc-KO cells were depleted to the same extent as in xCT-KO at 24-hours postseeding without NAC (Supplementary Fig. S3C). Also, these cells seem to be under oxidative (like xCT-KO cells) but not amino acid stress (unlike xCT-KO cells) based on the level of NRF2 and p-GCN2 levels, respectively. Furthermore, we compared lipid peroxide accumulation in GCLc-KO cells with xCT-KO cells and we found that in control conditions GCLc-KO cells indeed showed less accumulation of this ferroptotic marker in comparison with their xCT-KO counterparts 3 days postseeding. Expectantly, NAC succeeded to reverse the effect only in xCT-KO cells, whereas GSH was effective in both xCT- and GCLc-KO cells. Considering that accumulation of lipid peroxides was prominent in both xCT- and GCLc-KO cells it seems that the xCT-KO phenotype arises mainly from GSH scarcity. However, it appears that cysteine depletion in xCT-KO makes them more sensitive to ferroptosis. This comparison between xCT-KO and GCLc-KO cells deserves further attention in future studies.

Genetic disruption of xCT delays PDAC tumor xenografts

To further validate our *in vitro* xCT-KO results, we performed *in vivo* xenograft experiments. WT and xCT-KO cells of both cell lines treated with 1 µmol/L vitamin E were injected subcutaneously with Matrigel into nude mice and tumor growth was monitored. No tumor growth occurred for xCT-KO cells from both cell lines within 26 days (Fig. 4A, gray lines), while during this time the WT tumors had reached 1–1.5 cm^3 by day 18 (Capan-2) or day 26 (MiaPaCa-2; Fig. 4A, black lines). Use of Matrigel for cell injection enabled us to isolate the plugs remaining from MiaPaCa-2 xCT-KO cell injections to examine if the xCT-KO cells had survived during this period *in vivo* (square on the Fig. 4A). Surprisingly, after dissociating the Matrigel plugs and immersing them in media supplemented with NAC, we observed cells similar to MiaPaCa-2 xCT-KO mixed with dense stromal fibroblasts. Sequencing of genomic DNA from these cells and dependency of NAC for growth *in vitro* confirmed that these MiaPaCa-2 xCT-KO cells were viable *in vivo* after day 26 days (Fig. 4B and C).

The surprising finding that xCT-KO cells were able to survive for a long period *in vivo* led us to investigate if these cells were capable of forming tumors at a later time. Thus, we repeated the

A

Figure 3
Disruption of xCT in MiaPaCa-2 cells results in severe oxidative and amino acid stress. **A,** Relative intracellular GSH levels in MiaPaCa-2 and Capan-2 WT and xCT-KO (two independent clonal cell lines) cells, 24-hour postseeding in DMEM supplemented with 1 µmol/L vitamin E, 0.2 mmol/L or 1 mmol/L NAC. GSH content was normalized to the number of cells. Data shown represent the mean ± SEM; $n = 3$. *, $P < 0.05$, comparison with WT control cells. **B,** MiaPaCa-2 WT and xCT-KO cells were cultivated for 24 hours in DMEM supplemented or not with 1 µmol/L vitamin E, 1 mmol/L or 3 mmol/L NAC. Changes in phosphorylation status and protein abundance of members of the two major AA-sensing pathways GCN2 (p-GCN2/p-EIF2a/ATF4) and mTORC1 (p-S6K1 and p-RPS6) were analyzed by Western blot analysis. Blots are representative of three independent experiments.
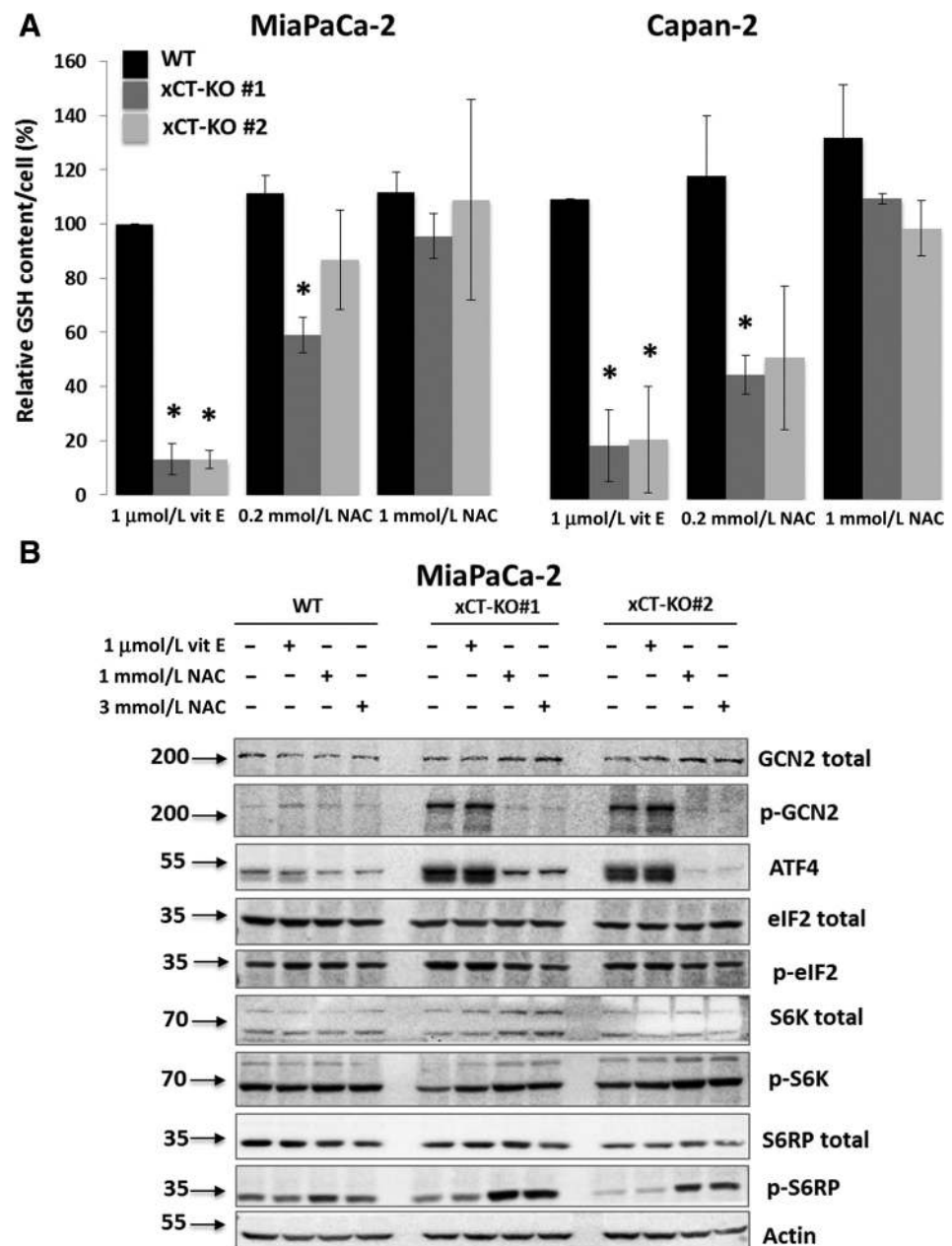
experiment and continued to observe mice injected with xCT-KO cells after WT tumors had reached maximal allowable size (∼3 weeks). As suspected, xCT-KO–derived tumors started to appear with an approximate delay of 2 weeks compared with WT cells. More surprisingly, when the xCT-KO tumors started to grow they reached maximal size (1 cm³) within 2 weeks, which mimicked the WT tumor growth rate (Supplementary Fig. S4). This important finding indicates that besides the key role played by the cystine transporter xCT, an additional cysteine homeostasis mechanism must operate *in vivo*. This is a key question that is addressed in the following section. Interestingly, orally-administrated NAC (40 mmol/L in drinking water based on previous reports; ref. 28) did not restore the growth observed with WT cells (Supplementary Fig. S4). A possible explanation may lie in the underexamined pharmacokinetics of orally administered NAC.

xCT-KO cells are capable of cysteine (CySH) uptake

It was surprising to observe that xCT-KO cells (of the highly *in vitro* sensitive MiaPaCa-2 cell line) can survive for a long period *in vivo* and eventually give rise to tumor formation (Supplementary Fig. S4). We postulated that the high *in vitro* sensitivity of xCT-KO cells might be due to cultivation in media (DMEM) exclusively containing the oxidized form of cysteine (CySSCy), while *in vivo* this is not the case. Therefore, we performed clonogenicity assays with MiaPaCa-2 WT and xCT-KO cells in DMEM containing different CySSCy-to-CySH ratios to test this hypothesis. Literature data vary regarding the precise ratio of these two cysteine forms, which can also be influenced by the redox state of the proximal tissues and blood *per se* (with CySSCy being the predominant form). Thus, we examined multiple ratios ranging from pure CySSCy to pure CySH forms. Interestingly, the viability,
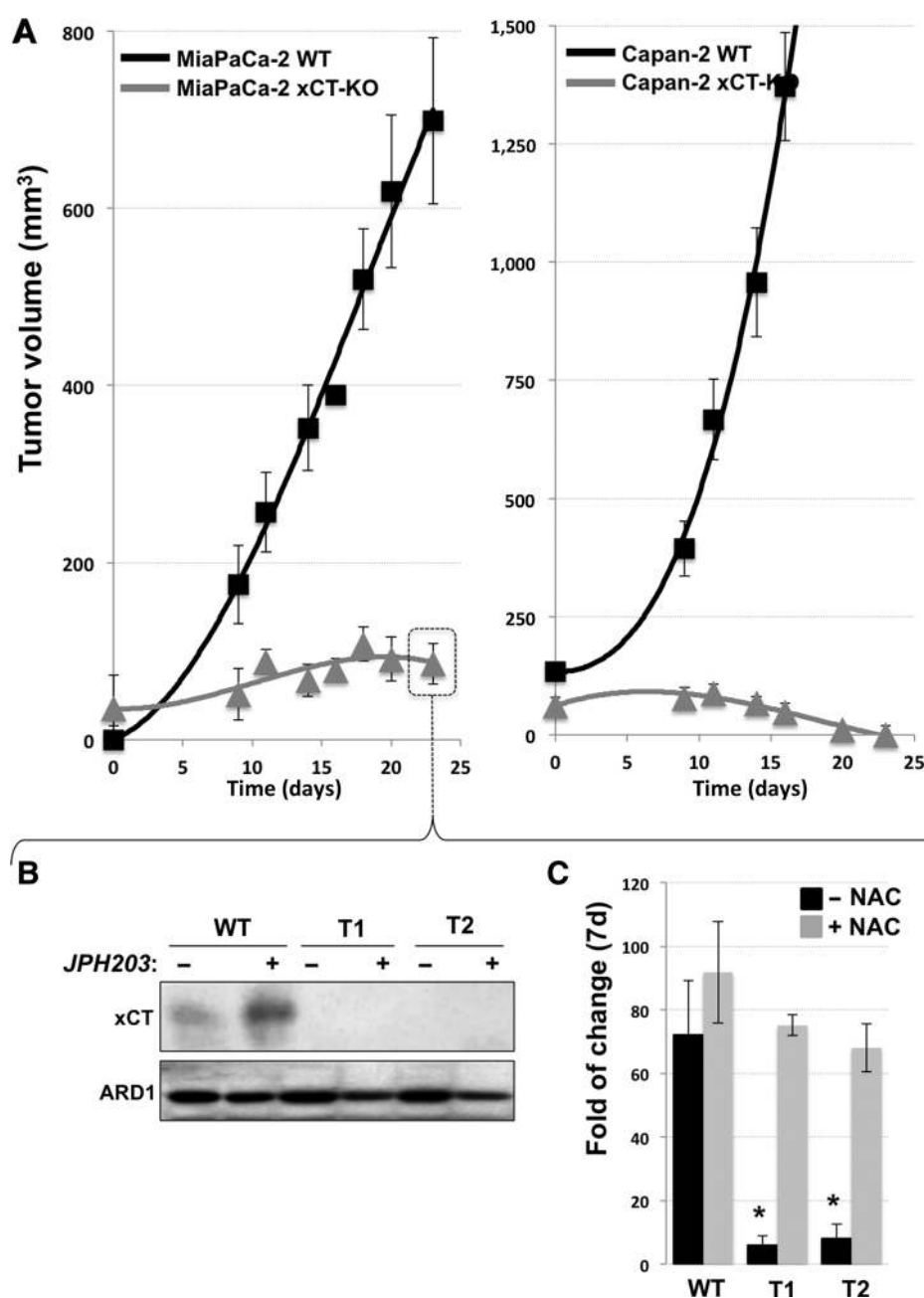
Figure 4
xCT is essential for tumor growth *in vivo*. **A,** Tumor volumes of WT and xCT-KO cells (MiaPaCa-2 and Capan-2) injected subcutaneously into nude mice showed severe inhibition of tumor growth upon xCT invalidation. **B,** No xCT protein band was detected in cells isolated from MiaPaCa-2 xCT-KO Matrigel plugs at the end of the experiment, even upon stimulation with JPH203 inhibitor. **C,** Seven-day proliferation of MiaPaCa-2 WT and isolated xCT-KO tumor cells in the presence and absence of 1 mmol/L NAC. Proliferation rate is presented as fold of change (mean $\pm$ SEM; $n = 3$; *, $P < 0.05$, comparison with WT control cells; Materials and Methods). ARD1 acted as a protein-loading control. Blots are representative of three independent experiments.

size, and number of colonies for xCT-KO cells completely correlated with the amount of CySH added (Fig. 5A, left). The biggest colonies, comparable to WT cells, were observed in media supplemented with CySH only. Under conditions where oxidized cysteine was present at 3 and 7 times more or as exclusively CySSCy, no visible xCT-KO colonies were observed after 7 days. However, when the experiment was prolonged for 10 additional days, lack of xCT-KO viable colonies was only observed with 100% CySSCy conditions (Fig. 5A, right). Seventeen-day clonogenicity assays were performed on both WT and xCT-KO cells but, except for the results presented in Fig. 5A, 17-day growth caused cells to reach confluency and die.

Following this, we investigated the influence of the same concentration of CySSCy, CySH, or NAC on the AA-sensing pathways in MiaPaCa-2 WT and xCT-KO cells. AA-homeostasis of WT cells was unaffected by any of these conditions during 24 hours. As expected, exclusive presence of CySSCy in media strongly compromised AA balance in xCT-KO cells as observed by upregulation of the active form of GCN2 and increased ATF4 expression (Fig. 5B) along with suppression of mTORC1 pathway components (phospho-S6K1 and phospho-S6RP). Furthermore, in these conditions xCT-KO cells showed increased expression of the transcription factor NRF2, suggesting an additional redox imbalance in the cells (although
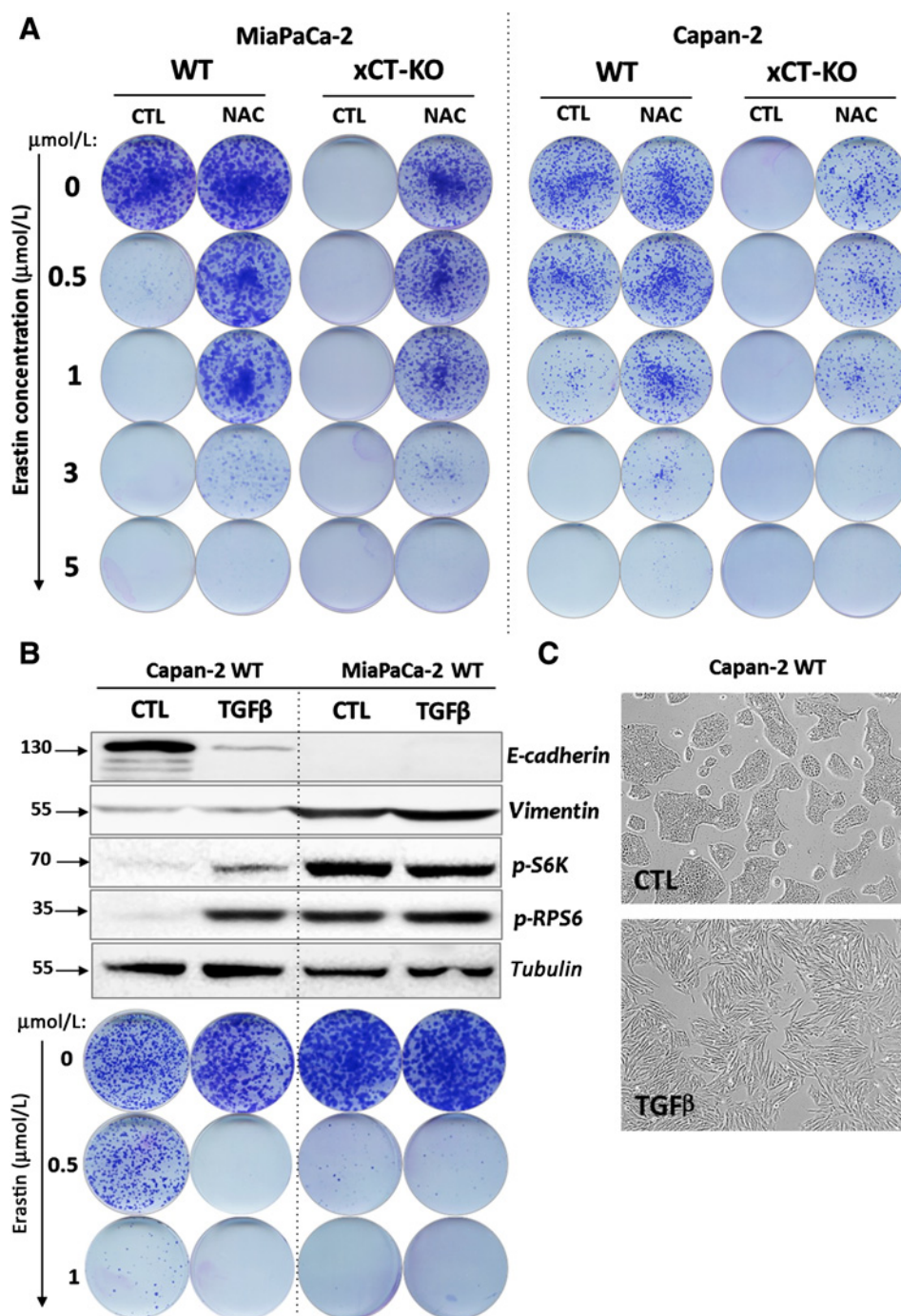
Figure 5
xCT-KO proliferation and survival depends on the presence of reduced form of cysteine. **A,** Clonal growth of MiaPaCa-2 WT and xCT-KO cells. Cells were cultivated 7 (left) or 17 (right) days in DMEM media supplemented with different concentrations of CySSCy/CySH (200:0; 175:25; 150:50; 100:100, 50:150, 0:200 µmol/L) and colored for visualization using Giemsa. Representative images are shown. **B,** The effects of different form of cyst(e)ine (final concentration 200 µmol/L) to amino acid and redox balance in MiaPaCa-2 WT and xCT-KO cells were investigated by immunoblotting, where relative protein contents of p-GCN2/ATF4 and p-S6K1/p-S6RP, as well as NRF2, were determined. ARD1 acted as a protein-loading control, and blots are representative of three independent experiments. #NB, the "200 µmol/L CySSCy" condition corresponds to the regular composition of DMEM media.
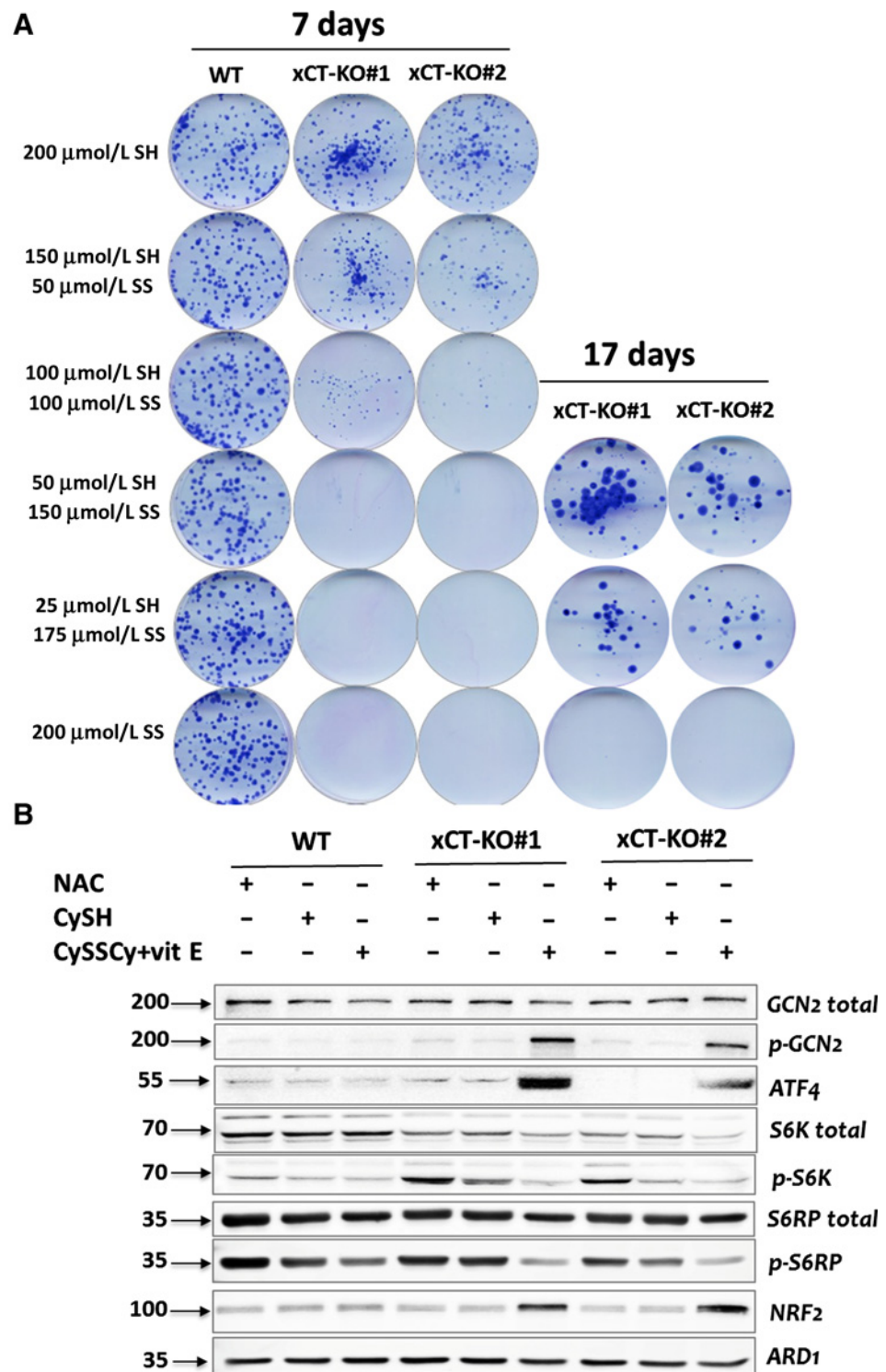
vitamin E was present and no lipid peroxides were detected previously in these conditions in xCT-KO cell lines). CySH presence, similar to NAC, restored both AA and redox balance in xCT-KO cells within 24 hours of cultivation (Fig. 5B). It is worth noting here that "media containing CySSCy" refers to the regular composition of DMEM.

Erastin phenocopies xCT-KO in PDAC WT cells only at low concentrations (1 µmol/L)

Taking advantage of the cells with genetically deleted xCT, we tested the sensitivity and specificity of the widely accepted xCT inhibitor—erastin (4, 9, 10, 29). WT and xCT-KO cells from both PDAC cell lines were treated with increasing inhibitor

Figure 6
The mesenchymal nature of MiaPaCa-2 cells makes them highly sensitive to xCT inhibition by erastin. **A,** Seven-day clonal growth of MiaPaCa-2 and Capan-2 WT and xCT-KO cells in the presence of different concentrations of erastin (0, 0.5, 1, 3, 5 µmol/L), supplemented or not with 1 mmol/L NAC. **B,** Relative protein content of E-cadherin and vimentin, as well as mTORC1 (p-S6K1 and p-RPS6), was determined in WT and xCT-KO of two PDAC cell lines upon TGFβ treatment for 48 hours. The effect of two different concentrations of erastin (0.5 and 1 µmol/L) on 7-day clonal growth of WT cells in the presence or absence of 10 ng/mL TGFβ was tested. Representative blots and images are shown. **C,** Micrographs show morphology of Capan-2 WT cells 48 hours after treatment or not with TGFβ.

concentrations (from 0 to 5 µmol/L). For MiaPaCa-2 cells, 0.5 µmol/L erastin was found to be selective as its suppressive effects on the clonogenicity potential were completely abolished by addition of NAC in both WT and xCT-KO cells (Fig. 6A, left). Erastin at 1 µmol/L in WT cells of both PDAC cell lines mimicked the genetic disruption of the xCT, and this effect was still reversible by the addition of NAC (Fig. 6A). Erastin at concentrations greater than 1 µmol/L were not reverted by the addition of NAC and more importantly killed xCT-KO cells growing with NAC showing that important off-target effects occur at these higher

doses (3 and 5 µmol/L). Interestingly, erastin in concentrations below 1 µmol/L did not suppress the clonogenicity potential of Capan-2 WT cells whereas it did for MiaPaCa-2 WT cells.

This approach was also utilized to test the specificity of 2 other commonly used inhibitors suggested to act by blocking xCT activity: sulfasalazine and sorafenib (Supplementary Fig. S5; ref. 9, 30). Unfortunately, we could not observe clear effects for these inhibitors. Namely, 0.5 mmol/L sulfasalazine disrupted Mia-PaCa-2 cells quite effectively and also Capan-2 cells to the much lesser extent (Supplementary Fig. S5, bottom). Conversely,

sorafenib showed a dose-dependent effect on proliferation for both cell lines, but no effect of simultaneous NAC-treatment was detected (Supplementary Fig. S5, top).

High sensitivity of MiaPaCa-2 to xCT inhibition: association with mesenchymal phenotype

Combined, the above results indicate that genetic disruption of xCT induces ferroptosis in both cell lines albeit with differing timing. Recently, studies have shown that different sensitivity toward ferroptosis might be the consequence of altered cellular states (31). To investigate this, we induced epithelial-to-mesenchymal transition (EMT) in Capan-2 WT cell line (showing prototypical markers of epithelial state—high expression of E-cadherin, as well as compact morphology) by treatment with TGFβ for 48 hours. TGFβ treatment substantially decreased expression of E-cadherin without a strong effect on the expression of mesenchymal marker—vimentin (Fig. 6B, Western analysis blots). These changes were also observed in the gross morphology as treated cells acquired mesenchymal-like status (Fig. 6C). Next, WT cells were treated with TGFβ, erastin, or their combination. TGFβ did not alter E-cadherin/vimentin expression in MiaPaCa-2 cells nor did it alter their sensitivity toward 2 different concentrations of erastin (Fig. 6B). However, TGFβ not only changed the morphology of the Capan-2 WT clones (making them more elongated), but also increased cellular sensitivity to inhibition of xCT by erastin by 2-fold. Erastin at 0.5 μmol/L, a concentration that alone is unable to substantially affect the clonogenicity potential of Capan-2 WT cells, when combined with TGFβ suppressed clonogenicity (Fig. 6B, bottom).

Interestingly, we observed an induction of mTORC1 (increased p-S6K1 and p-S6RP; Supplementary Fig. S6A), which could be a possible cause of increased sensitivity of TGFβ-treated Capan-2 cells to xCT inhibition. To investigate this, we treated highly sensitive MiaPaCa-2 xCT-KO cells with the inhibitor of protein synthesis (cycloheximide) for 24 hours and complete prevention of lipid peroxide accumulation was observed (Supplementary Fig. S6B), whereas the combinatory effect of TGFβ and erastin mimicked the kinetic of lipid peroxide accumulation (24 hours) and cell death (48 hours) in Capan-2 as in MiaPaCa-2 xCT-KO cells (Supplementary Fig. S6C and S6D). Our results provide strong support for previous work showing that a mesenchymal phenotype (especially ZEB1-driven) predicts high sensitivity to ferroptosis (32). However, based on the results obtained in Capan-2 xCT-KO cells (Fig. 1C, 2C, 3A, 4A; Supplementary Fig. S1–S3), an epithelial cell phenotype susceptibility to ferroptosis cannot be excluded, although the differences in timing of cell death and mechanisms involved in increased sensitivity requires further investigation.

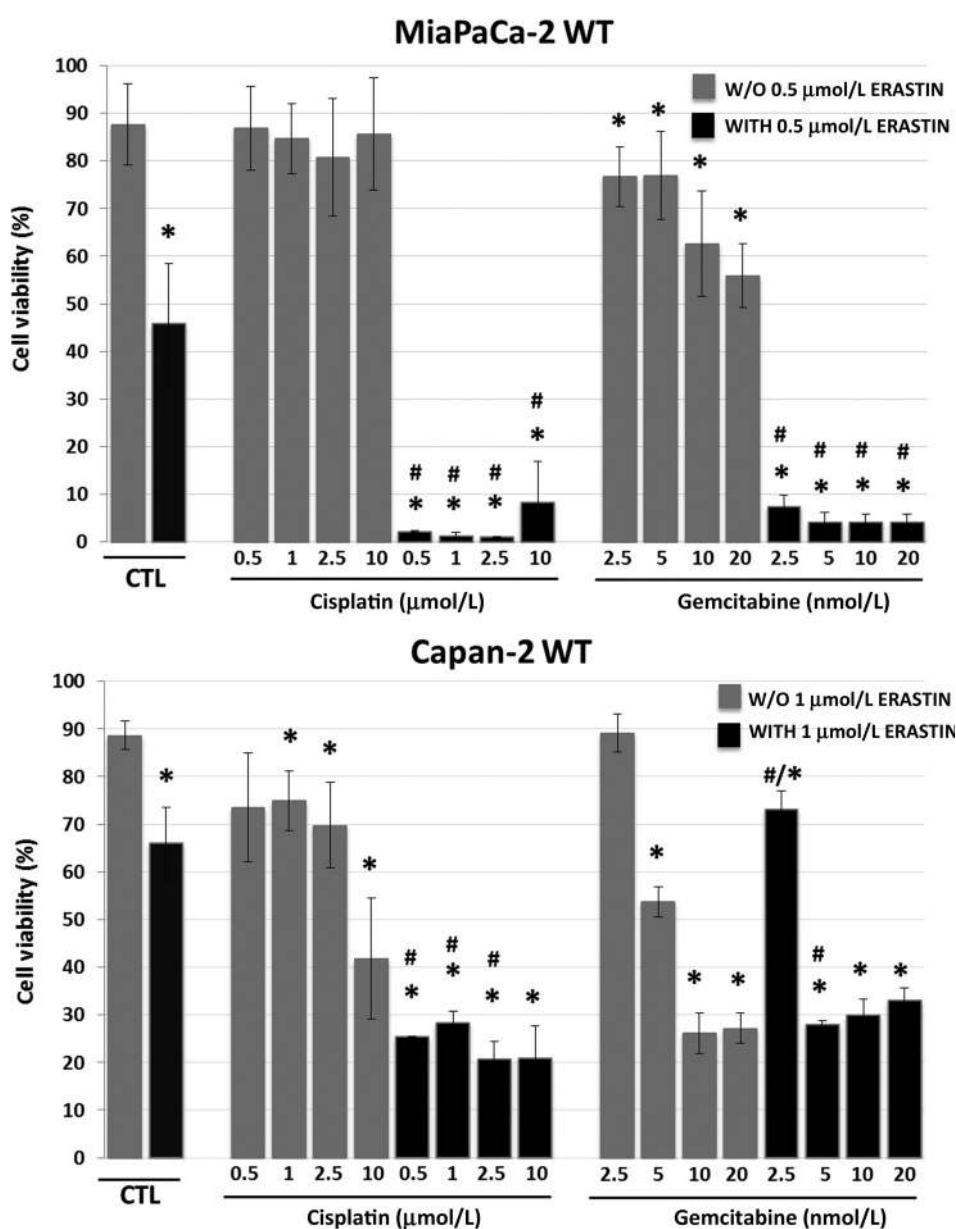### xCT inhibition potentiates cytotoxic effect of gemcitabine and cisplatin in both PDAC cell lines

Considering the key role of GSH in chemoresistance and the fact that xCT genetic disruption completely abolishes the cellular GSH pool, we analyzed the capacity of erastin to potentiate the cytotoxic effects of two widely used chemotherapeutics: cisplatin and gemcitabine (Fig. 7). Interestingly, combination of erastin with either cisplatin or gemcitabine at any examined concentration completely abolished cell survival. It is important to note here that the examined concentrations of chemotherapeutics had minimal effect on the MiaPaCa-2 cell survival alone, with the exception of 10 and 20 nmol/L gemcitabine (∼40% cell

death, Fig. 7, top). In Capan-2 cells, combined effects of 1 μmol/L erastin with cisplatin or gemcitabine were evident in lower doses of chemotherapeutics (0.5–2.5 μmol/L cisplatin and 2.5–5 nmol/L gemcitabine; Fig. 7, bottom). Interestingly, higher doses of chemotherapeutics (10 μmol/L for cisplatin, 10 and 20 nmol/L for gemcitabine) alone strongly compromised Capan-2 cell survival (∼60% cell death for cisplatin and ∼70% cell death for gemcitabine) and further decrease was not observed with erastin after 48 hours of treatment. NAC-treatment completely rescued the effects of erastin, erastin + cisplatin, and to a certain degree erastin + gemcitabine treatment, suggesting the important role that cysteine, and thus GSH, plays in the action of chemotherapeutics (Supplementary Fig. S7).

Discussion

Research during the past two decades has suggested an increasingly important role for CySSCy import via the system x_c^- in the maintenance of tumor cell growth, metastasis, and chemoresistance. Here, we evaluated this mechanism in one of the most aggressive cancers, PDAC, by genetic disruption of the xCT transport subunit. Interestingly, although previous work suggested that CySSCy can be imported via different transporters (25), xCT-KO showed a nearly complete (∼90%) abolishment of CySSCy import (Fig. 1B). Furthermore, xCT disruption completely suppressed cell proliferation (Figs. 1B; Supplementary Fig. S1B). These results combined with data obtained previously on LAT1 and ASCT2 (16–18, 33, 34) justify the widely accepted view that this "minimal set" of AA transporters in cancer is fundamental for the advanced proliferative phenotype of cancer cells (14–16). However, an important distinction in this regard is that xCT-KO strongly suppressed tumor cell survival *in vitro* (Fig. 2A; Supplementary Fig. S2A), which was not the case for KO of LAT1 and ASCT2 (17, 18). These results are in full agreement with recent pharmacologic studies showing inhibition of xCT with erastin as an inducer of ferroptotic tumor cell death (4, 9–12).

The term "ferroptosis" was born in 2012 when Stockwell's group described a new, iron-dependent, type of cell death (4). According to their hypothesis, the mild pro-oxidative state in cancer cells leads to oxidative damage of, among other things, membrane polyunsaturated fatty acids, and this is further propagated by the presence of ferrous irons (Fenton reaction; ref. 35). Considering that lipid peroxidation influences membrane permeability and thus cell integrity, accumulation of LOOH is strictly controlled by the GPx4 enzyme that removes LOOH using GSH as reducing power (8). This protective mechanism seems to be irreplaceable as its inhibition inevitably leads to accumulation of lipid peroxides and ferroptosis (8). Importantly, we observed that PDAC xCT-KO cell death was preceded by a complete collapse of GSH levels and a strong accumulation of LOOH (Fig. 2B; Supplementary Fig. S2B), suggesting that xCT is fundamental not only for the bulk of CySSCy import, but also for the overall cysteine and GSH pool in PDAC cells, and thus, GPx4 activity. NAC supplementation completely reversed the xCT-KO cellular phenotype. NAC transport across the membrane remains controversial, and in some cases has been proposed to not require a transport system (for further reading refer to ref. 26). Furthermore, the AA stress response observed in xCT-KO cells (activation of GCN2-ATF4; suppression of mTORC1) was completely restored by NAC supplementation (Fig. 3B; Supplementary Fig. S3B). Although NAC can serve as ROS-scavenger *per se* (26), our

MiaPaca-2 WT

Capan-2 WT

Figure 7

xCT inhibition strongly potentiates the cytotoxic effect of gemcitabine and cisplatin. MiaPaCa-2 and Capan-2 WT cells were seeded with erastin (0.5 and 1 μmol/L, respectively), cisplatin (0.5, 1, 2.5, or 10 μmol/L), gemcitabine (2.5, 5, 10, or 20 nmol/L) or a combination of erastin with either cisplatin or gemcitabine. Forty-eight-hour postseeding, cell viability was determined by the PI method using BD FACSMelody cytometer. These results represent the average of three independent experiments $\pm$ SEM. *, $P < 0.05$, comparison with control; #, $P < 0.05$, comparison between chemotherapy and corresponding (chemotherapy+erastin) groups.

results favor the hypothesis that NAC preferentially acts as an alternative donor of CySH for the xCT-KO cells, and not just as pure antioxidant for LOOH. Furthermore, 1 mmol/L NAC successfully restored GSH content in xCT-KO cells to control levels (Fig. 3A), which is most likely due to replenishment of the intracellular CySH pool. Conversely, the lipophilic antioxidant vitamin E also prevented (delayed) cell death and LOOH accumulation in xCT-KO cells (Fig. 2A and B; Supplementary Fig. S2A–S2D) but without restoring AA balance and intracellular GSH levels (Fig. 3; Supplementary Fig. S3B). The observed effect of vitamin E favors the hypothesis of a LOOH-dependent cell death in xCT-KO cells as it has been proven to potently suppress ferroptosis via removal of oxidative damage in the lipophilic cellular compartments (36). Combined, these results strongly suggest that xCT represents the most important transport system for extracellular CySSCy importation.

Tumor xenografts of xCT-KO cells did not grow during the 4-week period required for WT cell tumors to reach the maximal allowable size (Fig. 4). These results corroborate a very recent report of xCT-KO in a breast cancer cell (MDA-MB-231) xenografts (37). However, our ability to extract MiaPaCa-2 xCT-KO Matrigel cell plugs at the end of the experiment revealed that surprisingly, some of the injected xCT-KO cells had remained viable for more than 3 weeks. We confirmed that these MiaPaCa-2 xCT-KO cells were the same as those initially injected via genomic mutation sequencing and these cells maintained the same sensitivity towards NAC removal *in vitro* (Fig. 4B). These results suggest that cells did not acquire a CySSCy-dependent resistance mechanism during *in vivo* experimentation, such as upregulation of other CySSCy importer systems or enhancement of *de novo* CySH synthesis. Importantly, when we performed prolonged experiments, xCT-KO cells succeeded to form tumor xenografts

(Supplementary Fig. S4). It is worth noting here that Matrigel/cells injections in mice were supplemented with 1 µmol/L vitamin E to prevent xCT-KO cells engaging ferroptotic cell death at the time of injection into mice. A possible explanation for xCT-KO long-term cell survival and finally proliferation *in vivo* might be the presence of circulating CySH in the plasma. Also, CySH could be obtained *in vivo* from neighboring stromal cells (stromal cells were detected in our tumor extracts) as has been described for chronic lymphocytic leukemia cells expressing low levels of xCT (38). Namely, a widely overlooked concept in studies dealing with xCT is the fact that the vast majority of culturing media contain exclusively CySSCy, whereas CySH is present in only few routinely used media (e.g. Ham's F-12 media). CySSCy has been shown to be the predominant form of cysteine in human plasma, making approximately 60% to 85% of total cysteine (39, 40). However, this CySSCy-to-CySH ratio can be influenced by different conditions including diet, disease, smoking etc., but mostly in favor of CySSCy presence (39, 41). We explored this potential explanation and demonstrated that low CySH concentrations can indeed maintain viability of xCT-KO cells (see Fig. 5A for details). It is important to note here that we were also able to rescue xCT-KO cell growth *in vitro* when media containing CySSCy was supplemented with 80 µmol/L β-mercaptoethanol (Supplementary Fig. S1B), which according to Bannai (42) allows the reduction of extracellular CySSCy to CySH. Our *in vivo* results therefore unambiguously suggest that proliferation of PDAC xCT-KO cells is rather delayed; however, they also reveal that further investigation is required to understand at which extent reduced cysteine (present in low concentration *in vivo*, and rarely in the culturing media) may influence the physiology of xCT-KO cells and xCT pharmacologic inhibition.

Finally, to explore the future therapeutic potential of targeting xCT to improve chemosensitivity in PDAC cells, erastin treatment was combined with gemcitabine, the conventionally used chemotherapeutic agent, or cisplatin, the chemotherapeutic agent that has been proven to synergize with xCT inhibition in other cancer types (10, 43). Our results clearly suggest that the cytotoxic effect of both chemotherapeutic drugs were strongly potentiated in combination with the irreversible xCT inhibitor erastin (Fig. 7; ref. 10). These results support the concept that initial depletion of cellular antioxidant defense strategies can be highly beneficial for chemotherapy efficacy as xCT inhibition depleted the cellular GSH pool. GSH has been previously recognized as a key agent in cellular resistance toward cisplatin (for further reading refer to ref. 44), as well as gemcitabine (3). It is important to note that although inhibition of xCT *in vitro* has provided highly promising results, further precise pharmacokinetic and *in vivo* studies with erastin are required. This is critical as the clinical trial on glioma

with another xCT inhibitor, sulfasalazine, failed due to lack of response and severe side effects (45, 46).

Collectively, our results clearly show that xCT disruption in two different PDAC cell lines strongly affects their AA and redox balance, and thus suppresses *in vitro* and delays *in vivo* their proliferative phenotype. Importantly, unlike disruption of other essential AA-transporters such as LAT1 and ASCT2, xCT-KO enhanced susceptibility to cell death via ferroptosis. Increased sensitivity to xCT inhibition in cells with mesenchymal-like characteristics, which are the predominant cell type responsible for metastatic dissemination of PDAC (see ref. 47), suggest that xCT inhibitors are promising candidates for targeting vulnerability points in these highly aggressive tumors via the induction of ferroptosis.

Disclosure of Potential Conflicts of Interest

No potential conflicts of interest were disclosed.

Authors' Contributions

Conception and design: B. Daher, J. Durivault, J. Pouysségur, M. Vučetić
Development of methodology: B. Daher, S.K. Parks, J. Durivault, Y. Cormerais, J. Pouyssegur, M. Vucetic
Acquisition of data (provided animals, acquired and managed patients, provided facilities, etc.): B. Daher, J. Pouysségur, M. Vučetić
Analysis and interpretation of data (e.g., statistical analysis, biostatistics, computational analysis): B. Daher, S.K. Parks, J. Durivault, J. Pouysségur, M. Vučetić
Writing, review, and/or revision of the manuscript: B. Daher, S.K. Parks, Y. Cormerais, J. Pouysségur, M. Vučetić
Administrative, technical, or material support (i.e., reporting or organizing data, constructing databases): B. Daher, S.K. Parks, J. Durivault, Y. Cormerais, J. Pouysségur, M. Vučetić
Study supervision: J. Pouysségur, M. Vučetić
Other (xCT knockout of MiaPaca-2 WT cell line): H. Baidarjad
Other (L-[14C]-Leucine uptake): E. Tambutte

References

1. Siegel RL, Miller KD, Jemal A. Cancer statistics, 2016. CA Cancer J Clin 2016;66:7–30.
2. Balendiran GK, Dabur R, Fraser D. The role of glutathione in cancer. Cell Biochem Funct 2004;22:343–52.
3. Ju HQ, Gocho T, Aguilar M, Wu M, Zhuang ZN, Fu J, et al. Mechanisms of overcoming intrinsic resistance to gemcitabine in pancreatic ductal adenocarcinoma through the redox modulation. Mol Cancer Ther 2015;14: 788–98.
4. Dixon SJ, Lemberg KM, Lamprecht MR, Skouta R, Zaitsev EM, Gleason CE, et al. Ferroptosis: an iron-dependent form of nonapoptotic cell death. Cell 2012;149:1060–72.
5. Vucetic M, Cormerais Y, Parks SK, Pouyssegur J. The central role of amino acids in cancer redox homeostasis: vulnerability points of the cancer redox code. Front Oncol 2017;7:319.
6. Dix TA, Aikens J. Mechanisms and biological relevance of lipid peroxidation initiation. Chem Res Toxicol 1993;6:2–18.
7. Yang WS, SriRamaratnam R, Welsch ME, Shimada K, Skouta R, Viswanathan VS, et al. Regulation of ferroptotic cancer cell death by GPX4. Cell 2014;156:317–31.
8. Ursini F, Maiorino M, Valente M, Ferri L, Gregolin C. Purification from pig liver of a protein which protects liposomes and biomembranes from peroxidative degradation and exhibits glutathione peroxidase activity on

phosphatidylcholine hydroperoxides. Biochim Biophys Acta 1982;710: 197–211.

9. Dixon SJ, Patel DN, Welsch M, Skouta R, Lee ED, Hayano M, et al. Pharmacological inhibition of cystine-glutamate exchange induces endoplasmic reticulum stress and ferroptosis. eLife 2014;3: e02523.

10. Sato M, Kusumi R, Hamashima S, Kobayashi S, Sasaki S, Komiyama Y, et al. The ferroptosis inducer erastin irreversibly inhibits system xc- and synergizes with cisplatin to increase cisplatin's cytotoxicity in cancer cells. Sci Rep 2018;8:968.

11. Chen D, Fan Z, Rauh M, Buchfelder M, Eyupoglu IY, Savaskan N. ATF4 promotes angiogenesis and neuronal cell death and confers ferroptosis in a xCT-dependent manner. Oncogene 2017;36:5593–608.

12. Sehm T, Rauh M, Wiendieck K, Buchfelder M, Eyupoglu IY, Savaskan NE. Temozolomide toxicity operates in a xCT/SLC7a11 dependent manner and is fostered by ferroptosis. Oncotarget 2016;7:74630–47.

13. Bannai S, Kitamura E. Transport interaction of L-cystine and L-glutamate in human diploid fibroblasts in culture. J Biol Chem 1980;255:2372–6.

14. Barretina J, Caponigro G, Stransky N, Venkatesan K, Margolin AA, Kim S, et al. The Cancer Cell Line Encyclopedia enables predictive modelling of anticancer drug sensitivity. Nature 2012;483:603–7.

15. Bhutia YD, Babu E, Ramachandran S, Ganapathy V. Amino Acid transporters in cancer and their relevance to "glutamine addiction": novel targets for the design of a new class of anticancer drugs. Cancer Res 2015;75:1782–8.

16. McCracken AN, Edinger AL. Nutrient transporters: the Achilles' heel of anabolism. Trends Endocrinol Metab 2013;24:200–8.

17. Cormerais Y, Giuliano S, LeFloch R, Front B, Durivault J, Tambutte E, et al. Genetic disruption of the multifunctional CD98/LAT1 complex demonstrates the key role of essential amino acid transport in the control of mTORC1 and tumor growth. Cancer Res 2016;76:4481–92.

18. Cormerais Y, Massard PA, Vucetic M, Giuliano S, Tambutte E, Durivault J, et al. The glutamine transporter ASCT2 (SLC1A5) promotes tumor growth independently of the amino acid transporter LAT1 (SLC7A5). J Biol Chem 2018;293:2877–87.

19. van Geldermalsen M, Wang Q, Nagarajah R, Marshall AD, Thoeng A, Gao D, et al. ASCT2/SLC1A5 controls glutamine uptake and tumour growth in triple-negative basal-like breast cancer. Oncogene 2016;35:3201–8.

20. Schulte ML, Fu A, Zhao P, Li J, Geng L, Smith ST, et al. Pharmacological blockade of ASCT2-dependent glutamine transport leads to antitumor efficacy in preclinical models. Nat Med 2018;24:194–202.

21. Broer A, Fairweather S, Broer S. Disruption of amino acid homeostasis by novel ASCT2 inhibitors involves multiple targets. Front Pharmacol 2018;9: 785.

22. Bilton R, Mazure N, Trottier E, Hattab M, Dery MA, Richard DE, et al. Arrest-defective-1 protein, an acetyltransferase, does not alter stability of hypoxia-inducible factor (HIF)-1alpha and is not induced by hypoxia or HIF. J Biol Chem 2005;280:31132–40.

23. Ye P, Mimura J, Okada T, Sato H, Liu T, Maruyama A, et al. Nrf2- and ATF4-dependent upregulation of xCT modulates the sensitivity of T24 bladder carcinoma cells to proteasome inhibition. Mol Cell Biol 2014; 34:3421–34.

24. Wempe MF, Rice PJ, Lightner JW, Jutabha P, Hayashi M, Anzai N, et al. Metabolism and pharmacokinetic studies of JPH203, an L-amino acid transporter 1 (LAT1) selective compound. Drug Metab Pharmacokinet 2012;27:155–61.

25. McBean GJ, Flynn J. Molecular mechanisms of cystine transport. Biochem Soc Trans 2001;29:717–22.

26. Samuni Y, Goldstein S, Dean OM, Berk M. The chemistry and biological activities of N-acetylcysteine. Biochim Biophys Acta 2013;1830:4117–29.

27. Efeyan A, Comb WC, Sabatini DM. Nutrient-sensing mechanisms and pathways. Nature 2015;517:302–10.

28. Gao P, Zhang H, Dinavahi R, Li F, Xiang Y, Raman V, et al. HIF-dependent antitumorigenic effect of antioxidants in vivo. Cancer Cell 2007;12:230–8.

29. Dahlmanns M, Yakubov E, Chen D, Sehm T, Rauh M, Savaskan N, et al. Chemotherapeutic xCT inhibitors sorafenib and erastin unraveled with the synaptic optogenetic function analysis tool. Cell Death Discov 2017;3: 17030.

30. Gout PW, Buckley AR, Simms CR, Bruchovsky N. Sulfasalazine, a potent suppressor of lymphoma growth by inhibition of the x(c)- cystine transporter: a new action for an old drug. Leukemia 2001;15:1633–40.

31. Viswanathan VS, Ryan MJ, Dhruv HD, Gill S, Eichhoff OM, Seashore-Ludlow B, et al. Dependency of a therapy-resistant state of cancer cells on a lipid peroxidase pathway. Nature 2017;547:453–7.

32. Krebs AM, Mitschke J, Lasierra Losada M, Schmalhofer O, Boerries M, Busch H, et al. The EMT-activator Zeb1 is a key factor for cell plasticity and promotes metastasis in pancreatic cancer. Nat Cell Biol 2017;19: 518–29.

33. Broer A, Rahimi F, Broer S. Deletion of amino acid transporter ASCT2 (SLC1A5) reveals an essential role for transporters SNAT1 (SLC38A1) and SNAT2 (SLC38A2) to sustain glutaminolysis in cancer cells. J Biol Chem 2016;291:13194–205.

34. Scopelliti AJ, Font J, Vandenberg RJ, Boudker O, Ryan RM. Structural characterisation reveals insights into substrate recognition by the glutamine transporter ASCT2/SLC1A5. Nat Commun 2018;9:38.

35. Xie Y, Hou W, Song X, Yu Y, Huang J, Sun X, et al. Ferroptosis: process and function. Cell Death Differ 2016;23:369–79.

36. Yang WS, Stockwell BR. Synthetic lethal screening identifies compounds activating iron-dependent, nonapoptotic cell death in oncogenic-RAS-harboring cancer cells. Chem Biol 2008;15:234–45.

37. Cobler L, Zhang H, Suri P, Park C, Timmerman LA. xCT inhibition sensitizes tumors to gamma-radiation via glutathione reduction. Oncotarget 2018;9:32280–97.

38. Zhang W, Trachootham D, Liu J, Chen G, Pelicano H, Garcia-Prieto C, et al. Stromal control of cystine metabolism promotes cancer cell survival in chronic lymphocytic leukaemia. Nat Cell Biol 2012;14:276–86.

39. Droge W, Kinscherf R. Aberrant insulin receptor signaling and amino acid homeostasis as a major cause of oxidative stress in aging. Antioxidants Redox Signal 2008;10:661–78.

40. Brigham MP, Stein WH, Moore S. The concentrations of cysteine and cystine in human blood plasma. J Clin Invest 1960;39:1633–8.

41. Go YM, Jones DP. Cysteine/cystine redox signaling in cardiovascular disease. Free Radical Biol Med 2011;50:495–509.

42. Bannai S. [Use of 2-mercaptoethanol in cell culture]. Hum Cell 1992;5: 292–7.

43. Hagiwara M, Kikuchi E, Tanaka N, Kosaka T, Mikami S, Saya H, et al. Variant isoforms of CD44 involves acquisition of chemoresistance to cisplatin and has potential as a novel indicator for identifying a cisplatin-resistant population in urothelial cancer. BMC Cancer 2018;18:113.

44. Chen HH, Kuo MT. Role of glutathione in the regulation of Cisplatin resistance in cancer chemotherapy. Met-Based Drugs 2010;2010: 430939.

45. Robe PA, Martin D, Albert A, Deprez M, Chariot A, Bours V. A phase 1–2, prospective, double blind, randomized study of the safety and efficacy of Sulfasalazine for the treatment of progressing malignant gliomas: study protocol of [ISRCTN45828668]. BMC Cancer 2006;6:29.

46. Robe PA, Martin DH, Nguyen-Khac MT, Artesi M, Deprez M, Albert A, et al. Early termination of ISRCTN45828668, a phase 1/2 prospective, randomized study of sulfasalazine for the treatment of progressing malignant gliomas in adults. BMC Cancer 2009;9:372.

47. Wang S, Huang S, Sun YL. Epithelial-mesenchymal transition in pancreatic cancer: a review. BioMed Res Int 2017;2017:2646148.